Effect of electron count and chemical complexity in the Ta-Nb-Hf-Zr-Ti high-entropy alloy superconductor

Fabian von Rohr[a,1], Michał J. Winiarski[b], Jing Tao[c], Tomasz Klimczuk[b], and Robert Joseph Cava[a,1]

[a]Department of Chemistry, Princeton University, Princeton, NJ 08544; [b]Faculty of Applied Physics and Mathematics, Gdansk University of Technology, Gdansk 80-233, Poland; and [c]Condensed Matter Physics Department, Brookhaven National Laboratory, Upton, NY 11973

Contributed by Robert Joseph Cava, September 26, 2016 (sent for review July 28, 2016; reviewed by Jozef Spałek and Ronny Thomale)

High-entropy alloys are made from random mixtures of principal elements on simple lattices, stabilized by a high mixing entropy. The recently discovered body-centered cubic (BCC) Ta-Nb-Hf-Zr-Ti high-entropy alloy superconductor appears to display properties of both simple crystalline intermetallics and amorphous materials; e.g., it has a well-defined superconducting transition along with an exceptional robustness against disorder. Here we show that the valence electron count dependence of the superconducting transition temperature in the high-entropy alloy falls between those of analogous simple solid solutions and amorphous materials and test the effect of alloy complexity on the superconductivity. We propose high-entropy alloys as excellent intermediate systems for studying superconductivity as it evolves between crystalline and amorphous materials.

high-entropy alloys | superconductivity | disordered metals

Alloys are among the most relevant materials for modern technologies. Conventional alloys typically consist of one principal element, such as the iron in steel, plus one or more dopant elements in small proportion (e.g., carbon in the case of steel) that enhance a certain property of interest; the properties are based on the modification of those of the principal element. In sharp contrast, high-entropy alloys (HEAs) are composed of multiple principal elements that are all present in major proportion, with the simple structures observed attributed to the high configurational entropy of the random mixing of the elements on their lattice sites (1). Thus, the concept of a "principal element" becomes irrelevant. The elements in HEAs arrange on simple lattices with the atoms stochastically distributed on the crystallographic positions; HEAs are commonly referred to as metallic glasses on an ordered lattice (Fig. 1 *A* and *B*). The properties of HEAs arise as a result of the collective interactions of the randomly distributed constituents (2, 3). There is no strict definition, but HEAs are typically composed of four or more major elements in similar concentrations. By applying this concept, several new alloys with simple body-centered cubic (BCC), hexagonal closest-packing (HCP), or face-centered cubic (FCC) structures have been realized (2, 3, 4). The HEAs compete for thermodynamic stability with crystalline intermetallic phases with smaller numbers of elemental constituents (5). Therefore, one central concept of designing these alloys is to understand the interplay between mixing entropy ΔS_{mixing} and phase selection. Considering the large number of metals in the periodic table, the total number of possible HEA compositions is virtually unlimited.

In addition to their structural and chemical diversity, HEAs can display novel, highly tunable properties such as, for example, excellent specific strength (6, 7), superior mechanical performance at high temperatures (8), and fracture toughness at cryogenic temperatures (9, 10), making them promising candidates for new applications. Simple niobium–titanium-based binary alloys are nowadays still the most often and widely used materials for superconducting magnets, such as in NMR and MRI devices (11) or the Large Hadron Collider (12), and thus the discovery of bulk superconductivity with a single well-defined phase transition on a highly disordered BCC lattice in the Nb-Ti–related Ta-Nb-Hf-Zr-Ti HEA is of considerable interest (13, 14). This multicomponent phase, stabilized by the high mixing entropy, appears to fall between an ordered solid and a glass and thus allows for study of the chemical composition and structure–property relations of a superconducting material partway between an ordinary alloy and an amorphous material on a fundamental level. Here, we report the results of our investigations of the influence of electron count and alloy complexity on superconductivity in the Ta-Nb-Hf-Zr-Ti HEA. We find that the variation in superconducting transition temperature with electron count is intermediate to those displayed by simple alloys and amorphous materials and that the elemental makeup of the HEA superconductor is critical for determining its properties, despite the fact that the materials system is very highly disordered.

Results and Discussion

Structural Characterization of $[TaNb]_{1-x}(ZrHfTi)_x$. The powder X-ray diffraction (XRD) patterns of the HEAs $[TaNb]_{1-x}(ZrHfTi)_x$ for x = 0.2, 0.25, 0.3, 0.33, 0.35, 0.4, 0.45, 0.5, 0.6, 0.7, 0.8, and 0.84, which were synthesized by arc melting, can all be indexed with a simple BCC unit cell. [For better readability of the chemical formula, all elements with a valence electron count (VEC) of 5 are written in brackets, whereas elements with a VEC of 4 are written in parentheses throughout the article.] All prepared alloys fall within the definition for HEA compositions (2, 3), with no constituent element of less than 5 mol% and/or more than 40 mol%. In Fig. 1*C*, we show three representative XRD patterns of the members x = 0.3, 0.45, and 0.65. The patterns are found to shift only slightly with composition. Therefore, a shifting of the cell parameter a_0 is observed, but its change between the different HEAs is only minor. All alloys are found to be single phase with broad reflections, which we attribute to both the high degree of disorder present in the HEAs and the nonideal diffraction sample preparation (the alloys are too hard to crush by our methods, and so fine particle-size powders could not be made for the diffraction experiment). The observed

Significance

High-entropy alloys are a new class of materials that consist of several principal elements arranged on simple lattices. These structures are stabilized by the high configurational entropy of the random mixing of the elements. Here, we show that the properties of a superconducting high-entropy alloy are strongly related to the electron count and that the superconducting transition temperatures of these alloys fall between those of analogous crystalline and amorphous materials. We find that despite the large degree of randomness and disorder in these alloys, the superconducting properties are nevertheless strongly dependent on the chemical composition and complexity. We argue that high-entropy alloys are excellent model systems for understanding how superconductivity and other collective quantum states evolve from crystals to amorphous solids.

Author contributions: F.v.R. and R.J.C. designed research; F.v.R., M.J.W., J.T., and T.K. performed research; F.v.R., M.J.W., J.T., and T.K. analyzed data; and F.v.R. and R.J.C. wrote the paper.

Reviewers: J.S., Jagiellonian University; and R.T., Universität Würzburg.

The authors declare no conflict of interest.

[1]To whom correspondence may be addressed. Email: vonrohr@princeton.edu or rcava@princeton.edu.

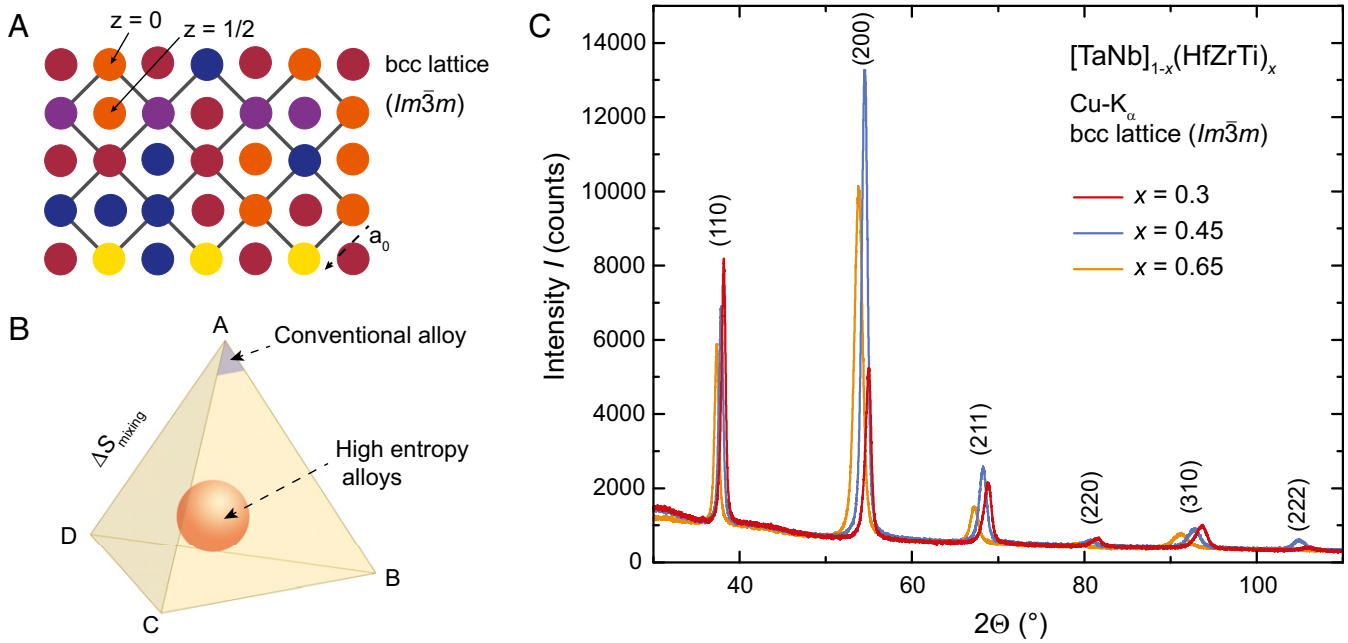

Fig. 1. (*A*) Schematic representation of a BCC lattice with randomly distributed atoms. (*B*) Schematic phase diagram of a multicomponent alloy system showing, schematically, conventional and HEA phase regions. (*C*) XRD patterns of the HEAs $[TaNb]_{1-x}(ZrHfTi)_x$ for $x = 0.3, 0.45, 0.65$.

unit cell change results from the large difference of atomic radii of the different constituent atoms. The unit cell parameter for the BCC lattice observed is found to vary from $a_0 \approx 3.33$ Å to 3.43 Å within the solid solution. The earlier reported cell parameter for variants of this Ta-Nb-Hf-Zr-Ti HEA follow this trend accordingly (13, 15). Thus, the observed physical properties reported below are those of the bulk, because no impurity phases are observed. An earlier-reported minor hexagonal phase impurity is not present in the samples of this study (15).

In Fig. 2, we show a representative high-resolution transmission electron microscope (HRTEM) image of a nearly optimally doped superconducting HEA sample $x = 0.33$. The HRTEM image is taken along the [111] zone axis. This image of the nanostructure of the alloy reveals the arrangement of the atoms on a simple, homogeneous BCC lattice, despite the presence of five constituent atoms with very different atomic radii. Critically, no nanoscale chemical phase separation was observed for any of the materials investigated. In Fig. 2, *Inset* we show the Fourier transform of the observed atom positions in the real space image. In the Fourier-transform pattern of the HRTEM image, the six reflections close to the center spot represent 110 planes, clearly supporting the BCC structure of the HEA even at the nanoscale.

The elemental metals in this pentinary superconducting HEA, when taken by themselves, order on either HCP or BCC lattices: whereas hafnium, zirconium, and titanium crystallize on a HCP lattice, niobium and tantalum crystallize on a BCC lattice at room temperature. For conventional alloys between metals with a VEC of 5 (niobium or tantalum) and with a VEC of 4 (titanium, zirconium, or hafnium) a structural transition from a HCP to BCC lattice is observed (16) with decreasing electron count. Due to their electron count, the HEAs prepared here with $x = 0.8$ and 0.84 would be expected to order on a HCP lattice. This polymorphic transition is, however, not observed in the HEA. The high entropy of the system therefore stabilizes the structure of this HEA preferentially on a BCC lattice (for example, refs. 16 and 17).

Electron-Count Dependence of the Superconductivity. In Fig. 3, we show the zero-field cooled (ZFC) magnetization of the HEAs $[TaNb]_{1-x}(ZrHfTi)_x$ with $x = 0.2, 0.25, 0.3, 0.33, 0.35, 0.4, 0.45, 0.5, 0.6, 0.7, 0.8$, and 0.84. The measurements were performed between 1.8 K and 9 K, with zero-field cooling and in an external field of $\mu_0 H = 2$ mT. For all samples a susceptibility larger than $\chi \approx -1$ (-1 is the ideal value for a fully superconducting material) below T_c was observed (the values more negative than $\chi = -1$ are caused by demagnetization effects). The temperature-dependent magnetizations are therefore plotted as $M(T)/M(0)$ for better comparability. The superconducting phase transitions of all samples are well defined in temperature. The critical temperatures T_c were determined as the values at the points where the linearly approximated slopes (dashed line) cross the normal state mag-

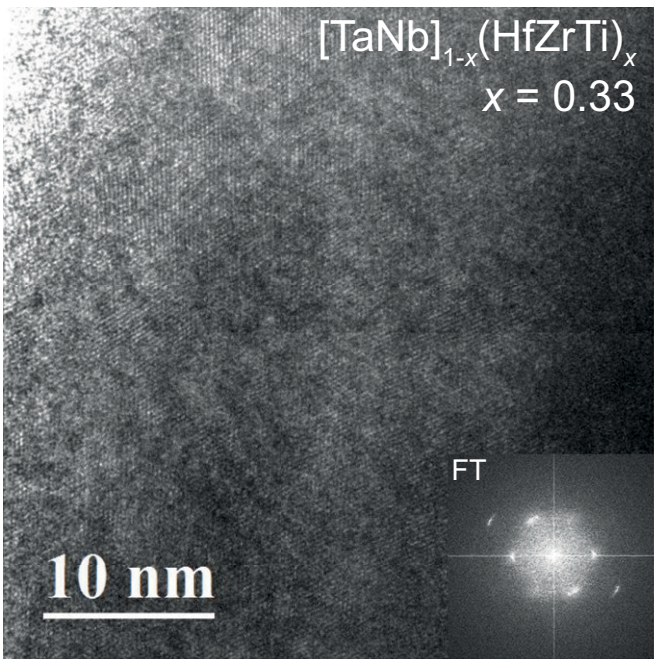

Fig. 2. Nanostructure of the HEA $[TaNb]_{1-x}(ZrHfTi)_x$ with $x = 0.33$ depicted in a HRTEM image. *Inset* shows the Fourier transformation of the observed real-space image of the BCC structure, in the [111] zone.

netization, illustrated by arrows in Fig. 3 for example for the sample $x = 0.6$. [No change in the general trend of critical temperatures is observed when the inflection point of the transition in $M(T)$is used to define T_c.] The critical temperatures T_c of the HEAs are plotted in Fig. 4 as a function of the electron/atom (e/a) ratio (purple squares, blue line is a trend line; for a review on electron counting, see ref. 18). For comparison the observed trend lines of the critical temperatures of the transition metals and their alloys in the crystalline form (19) (yellow dashed line in Fig. 4) and as amorphous vapor-deposited films (20) (red dashed line in Fig. 4) are also depicted. The trend of transition metals is often referred to as the Matthias rule, which links the T_c maxima with the noninteger d-electron count in simple binary alloys (19, 21). The trend line for amorphous superconductors is from the pioneering work of Collver and Hammond and coworkers (17, 20, 22), who studied the critical temperature T_c of vapor-cryodeposited films of transition-metal alloys and came to the conclusion that T_c vs. e/a ratio no longer exhibited the characteristic behavior of the Matthias rule for crystalline binary alloys. Instead they found that the critical temperatures T_c increase with increasing e/a, in a monotonic, rather structureless way with a maximum at a much higher e/a(d-electrons) = 6.4. These two curves, the Matthias rule, and the amorphous critical temperatures T_c after Collver and Hammond are the established standards to which other superconductors may be compared. Both of these trend lines have been the subject of extensive theoretical research as well (17).

The critical temperatures T_c of the HEA $[TaNb]_{1-x}(ZrHfTi)_x$ fall in between the two benchmark lines. The increase of the transition temperatures is clearly less pronounced than for crystalline alloys and follows rather a monotonically increasing trend as is observed for the amorphous superconductors. However, a maximum is reached near e/a(d-electrons) = 4.7, which is an essential feature of the Matthias rule, even though the maximum is much broader for the simple crystalline superconductors. Therefore, the great disorder of the HEA gives us the opportunity to investigate a superconducting system between the crystalline and amorphous benchmarks, with distinct features of both. Even though all chemical compositions used for this study are within a broad definition of HEAs (see above), the mixing entropy ΔS_{mixing} changes nevertheless across the series. The mixing entropy ΔS_{mixing} is estimated as is commonly done for HEAs assuming a mixture of hard spheres, in accordance with Mansoori and coworkers (2, 3, 23) The largest

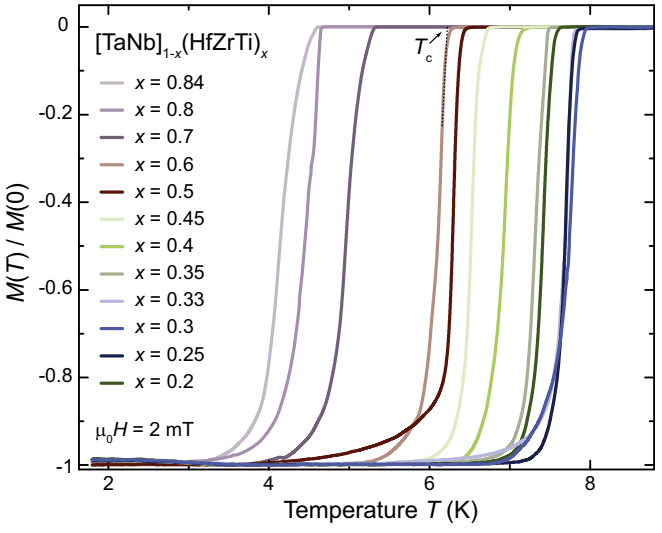

Fig. 3. Composition dependence of the superconducting transition in the Ta-Nb-Hf-Zr-Ti HEA. Shown is the ZFC magnetization of the HEAs $[TaNb]_{1-x}(ZrHfTi)_x$ with $x = 0.2, 0.25, 0.3, 0.33, 0.35, 0.4, 0.5, 0.6, 0.7, 0.8,$ and 0.84 in the vicinity of the superconducting transition, measured in an external magnetic field of $\mu_0 H = 2$ mT.

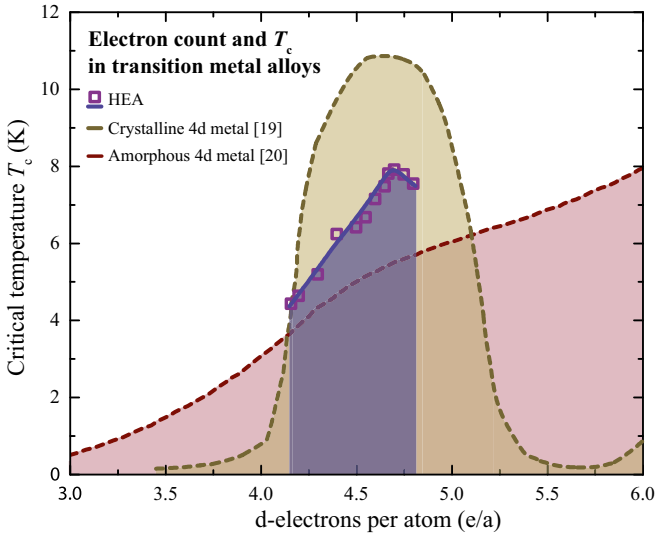

Fig. 4. Electron-count–dependent superconducting transition temperatures in the high-entropy alloy compared with those in analogous simple solid solution and amorphous phases. Shown is a phase diagram of $[TaNb]_{1-x}(ZrHfTi)_x$ (purple squares are the T_c and the blue line is a trend line) in comparison with transition metals and their alloys in the crystalline form (19) (yellow dashed line) and as amorphous vapor-deposited films (20) (red dashed line). The superconducting transition temperatures T_c are plotted as function of the electron/atom ratio.

mixing entropy ΔS_{mixing} is present at a ratio of e/a(d-electrons) = 4.4. The HEA series $[TaNb]_{1-x}(ZrHfTi)_x$ can therefore additionally be interpreted as a solid solution ranging from a higher-mixing entropy to a lower one. This may explain the general trends across the series: In the region of a more amorphous-like increase of the transition temperatures T_c the highest-mixing entropy is present, whereas in the region of the phase diagram with the lowest-mixing entropy a maximum of the transition temperatures T_c, which is in agreement with the Matthias rule, is observed.

Upper Critical Fields H_{c2} of the HEAs and the Effect of Increasing Mixing Entropy. In Fig. 5*A*, we show the temperature-dependent electrical resistivity ρ of the HEA $[TaNb]_{1-x}(ZrHfTi)_x$ with $x = 0.5$ in a temperature range between $T = 2$ K and 300 K. The resistivity at room temperature exhibits a value of $\rho(300\ K) \approx 116\ \mu\Omega$cm. The resistivity is found to be metallic and decreasing linearly with decreasing temperature. The residual resistivity ratio (RRR), $RRR = \rho(300\ K)/\rho(8\ K)) \approx 1.1$, is a low value, comparable to that observed for nonstoichiometric or highly disordered intermetallic compounds. The linear behavior of $\rho(T)$ is also a common behavior for highly disordered alloys, caused by the short lifetimes of the quasiparticles, which are scattered by the disorder and therefore decohere. This kind of conductivity is generally referred to as "bad metal conductivity." It is also found in strongly correlated materials such as the high-T_c superconductors and in transition metal systems, e.g., VO_2 (24, 25). In Fig. 5*A*, *Inset* the magnetic field dependence of the resistivity in the vicinity of the superconducting phase transition is shown for the sample with $x = 0.5$, for magnetic fields between $\mu_0 H = 0$–9 T in 0.5-T steps. The transition temperature T_c is reduced with increasing field H. The superconductivity is at 9 T still observable above $T = 2$ K, indicating a high upper critical field $\mu_0 H_{c2}(0)$. [The upper critical fields were determined by the 50% criterion; i.e., the upper critical field $\mu_0 H_{c2}(T)$ is defined by the temperature T at which 50% of the normal-state resistivity is suppressed, illustrated by the dashed line in Fig. 5*A* (e.g., refs. 26–28)]. In Fig. 5*B*, the temperature dependence of the upper critical fields $\mu_0 H_{c2}(T)$ of the HEAs $[TaNb]_{1-x}(ZrHfTi)_x$ with $x = 0.30$, 0.33, 0.35, 0.5, and 0.84 is shown. The dashed lines in Fig. 5*B*

represent the slopes of the upper critical fields $(dH_{c2}/dT)_{T=T_c}$ for all five samples, respectively. These slopes are used to estimate the upper critical fields at zero temperature $\mu_0 H_{c2}(0)$ by applying the Werthamer–Helfand–Hohenberg (WHH) approximation in the dirty limit (29), according to

$$H_{c2}^{WHH}(0) = -0.69\ T_c \left(\frac{dH_{c2}}{dT}\right)_{T=T_c}. \quad [1]$$

The obtained critical temperatures (from the resistivity measurements), the slopes of the upper critical fields $(dH_{c2}/dT)_{T=T_c}$, and estimated values after WHH approximation of the upper critical fields at zero temperature $\mu_0 H_{c2}^{WHH}(0)$ are summarized in Table 1. It is noteworthy that the slopes of the upper critical field increase with increasing mixing entropy of the system. Therefore, it is not the member of this series with the highest critical temperature T_c that has the largest $\mu_0 H_{c2}(0)$. Rather, the sample $x = 0.5$ has the largest upper critical field with a large negative slope of the upper critical field $(dH_{c2}/dT)_{T=T_c} \approx -2.618$ T/K and an overall upper critical field $\mu_0 H_{c2}(0) \approx 11.67$ T. This value is very close to the Pauli paramagnetic limit $\mu_0 H_{c2}^{Pauli} = 1.84\ T_c = 11.9$ T. For the sample with $x = 0.84$, the slope of the upper critical field is $(dH_{c2}/dT)_{T=T_c} \approx -2.893$ T/K, the largest in absolute value. This sample is also the one with the largest mixing entropy ΔS_{mixing} among the investigated alloys. For $x = 0.84$, the experimentally observed upper critical field $\mu_0 H_{c2}(0)$ is even found to exceed the Pauli paramagnetic limit $\mu_0 H_{c2}^{Pauli} = 1.84\ T_c = 8.3$ T. Therefore, strong spin-orbit coupling may play a role in the characteristic properties of the superconducting state in these HEAs. The observed systematic change of $\mu_0 H_{c2}(0)$ does not, however, correlate with the atomic spin-orbit coupling, which does not change much in the series, and therefore a relationship between $\mu_0 H_{c2}(0)$ and the magnitude of spin-orbit coupling cannot be established here.

Table 1. Critical temperatures T_c, slopes of the upper critical fields $(dH_{c2}/dT)_{T=T_c}$, and upper critical fields at zero temperature $\mu_0 H_{c2}^{WHH}(0)$ of $[TaNb]_{1-x}(ZrHfTi)_x$ with $x = 0.3$, 0.33, 0.4, 0.5, and 0.84

$[TaNb]_{1-x}(ZrHfTi)_x$	T_c (resistivity), K	$\left(\frac{dH_{c2}}{dT}\right)_{T=T_c}$, T/K	$\mu_0 H_{c2}^{WHH}(0)$, T
$x = 0.3$	8.03	−1.203	6.67
$x = 0.33$	7.75	−1.449	7.75
$x = 0.4$	7.56	−1.616	8.43
$x = 0.5$	6.46	−2.618	11.67
$x = 0.84$	4.52	−2.893	9.02

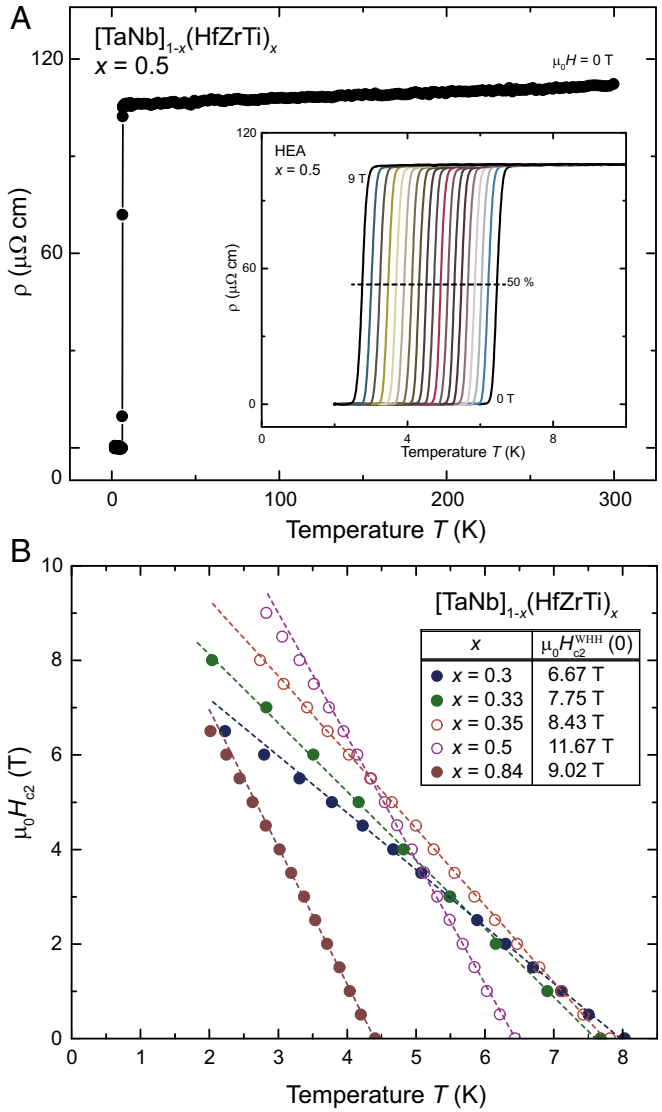

Fig. 5. (*A*) Resistivity between 2 K and 300 K of the HEA $[TaNb]_{1-x}(ZrHfTi)_x$ with $x = 0.5$. *A*, *Inset* shows the magnetic field dependence of the superconducting transition in fields from $\mu_0 H = 0$ T to 9 T in steps of 0.5 T. The dotted line displays the 50% criterion, which is commonly used for the determination of the upper critical field H_{c2}. (*B*) Temperature dependence of the upper critical field H_{c2}, determined by the 50% criterion, of the $[TaNb]_{1-x}(ZrHfTi)_x$ HEAs with $x = 0.30$, 0.33, 0.35, 0.5, and 0.84. The lines are linear fits for determination of $(dH_{c2}/dT)_{T=T_c}$.

The mixing entropy ΔS_{mixing} can be reduced either by the method described above or by the reduction of the number of constituent atoms of the alloy. We have prepared seven alloys for comparison, close to the optimal valence electron concentration of e/a(d-electron) = 4.7. These alloys are all found to randomly arrange on BCC lattices, as expected (e.g., refs. 17 and 30). In Fig. 6, we show the ZFC magnetization of the alloys $[TaNbV]_{0.67}(ZrHfTi)_{0.33}$, $[TaNb]_{0.67}(ZrHfTi)_{0.33}$, $[TaV]_{0.67}(ZrHfTi)_{0.33}$, $[NbV]_{0.67}(ZrHfTi)_{0.33}$, $[Nb]_{0.67}(ZrHfTi)_{0.33}$, $[TaNb]_{0.67}(ZrHf)_{0.33}$, and $[TaNb]_{0.67}(Hf)_{0.33}$ in the vicinity of the superconducting transition measured in an external field of $\mu_0 H = 2$ mT. The critical temperature T_c is found to decrease very little on going from the binary alloy $[Nb]_{0.67}(Ti)_{0.33}$, with a critical temperature of $T_c \approx 9.2$ K (19, 30), to the HEA $[TaNb]_{0.67}(ZrHfTi)_{0.33}$, where the atoms are highly disordered. The disorder introduced by the increasing number of constituent atoms does not lead to a loss of the superconductivity or to a very large decrease of the critical temperatures T_c. It is also apparent that the superconducting properties of these alloys are not just a compositional mixture of all of the properties of the constituent elements, but rather that a single homogeneous superconducting phase is observed for all of them; the highly disordered atomic content of the alloy conspires to give rise to one homogeneous superconducting state. In this sense superconductivity in the HEA is a logical further development of transition-metal alloys consisting of constituent atoms with a VEC of 4 and 5. The critical temperature decreases to $T_c \approx 4.2$ K for $[TaNbV]_{0.67}(ZrHfTi)_{0.33}$ indicates that the elemental makeup is significant for the physical properties even for the highly disordered atoms on simple lattices in HEAs.

Electron–Phonon Coupling in the HEA Superconductor. We have performed specific heat measurements on $[TaNb]_{0.67}(ZrHfTi)_{0.33}$, $[TaNb]_{0.16}(ZrHfTi)_{0.84}$, and $[TaNbV]_{0.67}(ZrHfTi)_{0.33}$, to get further insights into the nature of the different critical temperatures T_c that are the result of varying electron count and elemental composition of the alloys. In Fig. 7, we show the temperature-dependent specific heat capacities in fields from $\mu_0 H = 0$ T to 8 T in the vicinity of the superconducting phase transition of the three alloys. All three alloys display a single well-defined transition, which is further evidence for the emergence of a single collective

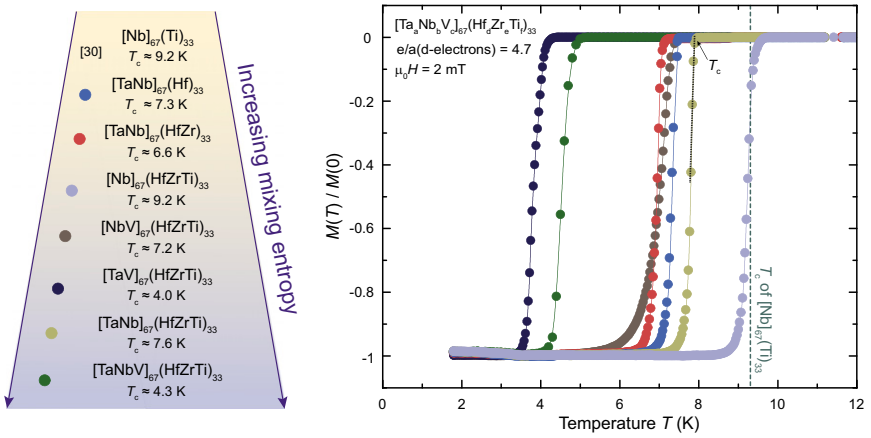

Fig. 6. The effect of alloy complexity on the superconducting transition. Shown is the ZFC magnetization in an external field of $\mu_0 H = 2$ mT of the alloys $[TaNb]_{0.67}(ZrHfTi)_{0.33}$, $[Nb]_{0.67}(ZrHfTi)_{0.33}$, $[TaNb]_{0.67}(ZrHf)_{0.33}$, $[TaNb]_{0.67}(Hf)_{0.33}$, and $[TaNbV]_{0.67}(ZrHfTi)_{0.33}$ in the vicinity of the superconducting transition.

superconducting phase. The normal-state contribution has been fitted to the data at low temperatures (dotted lines) according to

$$\frac{C(T)}{T} = \gamma + \beta T^2, \qquad [2]$$

with the Sommerfeld constant γ and $\beta = 12\pi^4 nR/5\Theta_D^3$, where n is the number of atoms per formula unit, $R = 8.31$ J·mol^{-1}·K^{-1} is the gas constant, and Θ_D is the Debye temperature. For comparability reasons the number of atoms per formula unit n was fixed to be 100. The obtained values for γ, β, and Θ_D are summarized in Table 2. The obtained ratios $\Delta C/\gamma T_c$ all exceed the standard weak-coupling BCS value, which is $\Delta C/\gamma T_c = 1.43$, indicating intermediate- to strong-coupling superconductivity. The Sommerfeld constant is found to decrease substantially from $\gamma \approx 797$ mJ·mol^{-1}·K^{-2} to 645 mJ·mol^{-1}·K^{-2} with a decreasing electron count within the series $[TaNb]_{1-x}(ZrHfTi)_x$. Thereby, the density of states at the Fermi level is reduced, because γ is proportional to the density of states at the Fermi level ($\gamma \propto D(E_F)$). Thus, we attribute the decreasing of the critical temperature T_c with an increasing electron count to a significant decrease in the density of states. It should be noted that simultaneously also the electron–phonon coupling is lowered, which also might contribute to the lowering of the critical temperature (see below). $[TaNb]_{0.67}(ZrHfTi)_{0.33}$ and $[TaNbV]_{0.67}(ZrHfTi)_{0.33}$ have nominally the same electron count, and experimentally we find the same density of states at the Fermi level, with almost identical values for γ. The Debye temperature is found to increase only slightly. Thus, although the critical temperatures differ by almost a factor of 2, there is not much difference in the fundamental quantities that determine the transition temperature: γ and Θ_D. We therefore tentatively attribute the decrease in T_c to the difference in the electron–phonon coupling λ that must occur on going from $[TaNb]_{0.67}(ZrHfTi)_{0.33}$ to $[TaNbV]_{0.67}(ZrHfTi)_{0.33}$. The electron–phonon coupling λ_{el-ph} can be estimated using the approximated McMillan formula, which is based on the phonon spectrum of niobium (31, 32) and is valid for $\lambda < 1.25$ (33):

$$\lambda_{el-ph} = \frac{1.04 + \mu^* \ln\left(\frac{\Theta_D}{1.45T_c}\right)}{(1 - 0.62\mu^*)\ln\left(\frac{\Theta_D}{1.45T_c}\right) - 1.04}. \qquad [3]$$

The parameter μ^* is the effective Coulomb repulsion that arises from Coulomb-coupling propagating much more rapidly than phonon coupling. Here, we use a value of $\mu^* = 0.13$, which is an average value used commonly for intermetallic superconductors (e.g., ref. 34). Having the Sommerfeld parameter and the electron–phonon coupling, the noninteracting density of states at the Fermi energy can be calculated according to

$$D(E_F) = \frac{3\gamma}{\pi^2 k_B^2 (1 + \lambda_{el-ph})}. \qquad [4]$$

From the electronic low temperature-specific heat data, we have estimated the value of the superconducting gap of all three compounds, according to

$$C_{el} = a\ exp(-\Delta(0)/k_B T_c). \qquad [5]$$

The obtained values for the electronic and phononic contributions to the superconductivity in HEAs are summarized in Table 2. The values for $\Delta(0)$ are similar to those of comparable intermetallic

Table 2. Summary of the electronic and phononic contributions to the superconductivity in the HEAs

Specific heat parameters	$[TaNb]_{0.67}(ZrHfTi)_{0.33}$	$[TaNb]_{0.16}(ZrHfTi)_{0.84}$	$[TaNbV]_{0.67}(ZrHfTi)_{0.33}$
T_c, K	7.70	4.59	4.11
γ, mJ·mol^{-1}·K^{-2}	7.97(5)	6.45(8)	7.97(4)
β, mJ·mol^{-1}·K^{-4}	0.170(4)	0.311(9)	1.48(5)
Θ_D, K	225(2)	184(2)	236(3)
λ_{el-ph}	0.83	0.73	0.65
$D(E_F)$, st. eV^{-1}/at. f.u.	1.9	1.6	2.1
$\Delta C/\gamma T_c$	1.89	1.98	1.62
$\Delta(0)$, meV	1.21(2)	0.71(1)	0.56(1)
$2\Delta(0)/k_B T_c$	3.7	3.6	3.2

The error of the fit of the specific heat is given in parentheses. st. eV^{-1}/at. f.u., states in eV^{-1} per atomic formula unit.

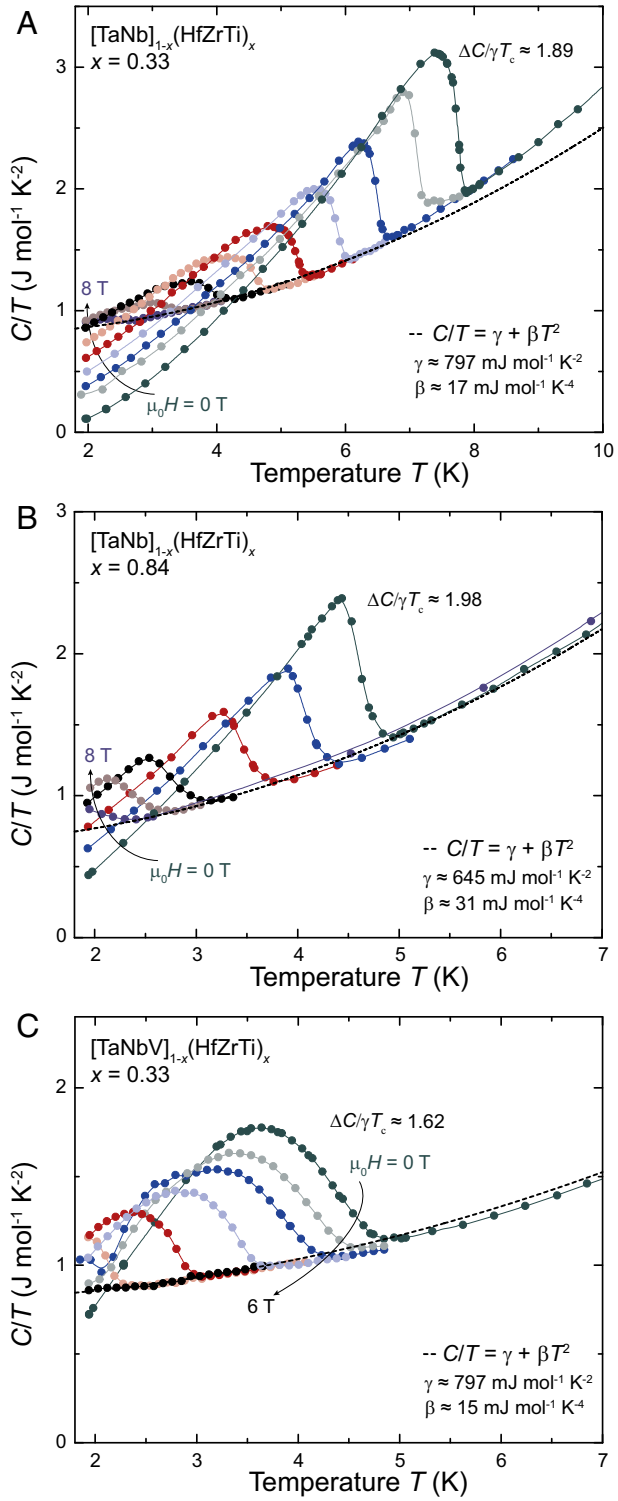

Fig. 7. Specific heat measurements in fields from $\mu_0 H = 0$ T to 8 T in the vicinity of the superconducting phase transition, for three representatives samples: (*A*) the nearly optimally doped HEA $[TaNb]_{1-x}(ZrHfTi)_x$ with $x = 0.33$; (*B*) the HEA with $x = 0.84$, which has a upper critical field $\mu_0 H_{c2}$ above the Pauli limit; and (*C*) the nearly optimally doped HEA $[TaNbV]_{1-x}(ZrHfTi)_x$, which includes vanadium, with $x = 0.33$; the T_c for this HEA is significantly lower than for the equivalent electron-count HEA where vanadium is not present.

superconductors and for all three samples the value for $2\Delta(0)/k_B T_c$ is close to the expected value of 3.52, which is expected for s-wave superconductors according to the BCS model. The estimated values for the electron–phonon coupling λ_{el-ph} further support that the density of states at the Fermi level $D(E_F)$ remains the same for $[TaNb]_{0.67}(ZrHfTi)_{0.33}$ and $[TaNbV]_{0.67}(ZrHfTi)_{0.33}$, whereas the electron–phonon coupling constant λ_{el-ph} is strongly reduced for the latter material. This finding supports the general concept that specific elements are essential for optimized superconductivity in compounds. Here we find that the elemental makeup is crucial even in the case of a highly disordered multicompontent HEA superconductor.

Summary and Conclusion

We have synthesized the HEA $[TaNb]_{1-x}(ZrHfTi)_x$ for $x = 0.2$, 0.25, 0.3, 0.33, 0.35, 0.4, 0.45, 0.5, 0.6, 0.7, 0.8, and 0.84 by arc melting of the elements under argon and by subsequent quenching. We found from X-ray powder diffraction measurements that all these alloys arrange on a simple BCC crystal lattice ($Im\bar{3}m$), with unit cell parameters between $a_0 \approx 3.33$ Å and 3.43 Å within the solid solution. All prepared samples are found to be bulk superconductors with critical temperatures between $T_c \approx$ 4.49 K and 7.92 K. By comparison of the critical temperatures of $[TaNb]_{1-x}(ZrHfTi)_x$ with the critical temperatures of the transition metals and their alloys in the crystalline form and as amorphous vapor-deposited films, we find the superconducting HEA to display characteristics intermediate to both of them. The valence electron dependence of the transition temperatures for $[TaNb]_{1-x}(ZrHfTi)_x$ is clearly less pronounced than that seen for crystalline alloys. However, a maximum is reached around e/a(d-electron) = 4.7, which is an essential feature of the Matthias rule for crystalline transition metal superconductors. Therefore, we find that this system follows neither a crystalline nor an amorphous-like trend for this collective electron state. We find the temperature-dependent electrical resistivity ρ of the HEAs $[TaNb]_{1-x}(ZrHfTi)_x$ to be metallic and decreasing linearly with decreasing temperature and that the slopes of the upper critical field $(dH_{c2}/dT)_{T=T_c}$ increase with increasing mixing entropy of the system. It is, therefore, not the member of this series with the highest critical temperature T_c that has the largest $\mu_0 H_{c2}(0)$. Rather, the sample with $x = 0.5$ has the largest upper critical field, with a large negative slope of the upper critical field $(dH_{c2}/dT)_{T=T_c} \approx -2.618$ T/K and an overall $\mu_0 H_{c2}(0) \approx 11.67$ T. By reducing the mixing entropy ΔS_{mixing} the critical temperatures are found to decrease only slightly from the binary alloy $[Nb]_{0.67}(Ti)_{0.33}$ with a critical temperature of $T_c \approx 9.2$ K to the HEA $[TaNb]_{0.67}(ZrHfTi)_{0.33}$. Thus, the disorder introduced by the increasing number of constituent atoms does not lead to a loss of the superconductivity or a large decrease of the critical temperature T_c. We do find, however, that the effect of elemental makeup is significant for the physical properties even for the highly disordered atoms on the simple lattice in this superconducting HEA. The general interplay of chemical structure, disorder, and superconductivity is a topic of fundamental interest. Many known superconductors are posed near structural instabilities, for example, the bismuth oxide superconductors (35, 36), the tungsten bronzes (37), and also many intermetallic superconductors (38, 39). The superconducting HEA studied here offers the unique opportunity to investigate superconductivity on one of the three most fundamental crystal lattices stabilized by high-entropy mixing. Our results suggest that HEAs are versatile model systems for the investigation of structure–property relations, as well as for the understanding of the change of electronic properties, going from crystalline to amorphous superconducting materials.

Methods

All samples were prepared from pieces of the pure metals. Stoichiometric amounts of niobium (purity 99.8%), tantalum (purity 99.9%), zirconium (purity 99.6%), hafnium (purity 99.6%), and titanium (purity 99.95%) pieces were arc melted in high currents ($T > 2{,}500°$ C) in an argon atmosphere and rapidly cooled on a water-chilled copper plate. A zirconium sponge was coheated to

purify the reaction atmosphere from remaining oxygen. The samples were melted five times and turned over each time to ensure optimal mixing of the constituents; the weight loss during melting was found to be insignificant. X-ray diffraction patterns were obtained from mechanically flattened pieces (in liquid nitrogen) of the very hard alloys, measured in a Bragg–Bretano reflection geometry. The patterns were obtained on a Bruker D8 Advance Eco with Cu K_α radiation and a LynxEye-XE detector. The resistivity, magnetization, and specific heat were studied using a Quantum Design physical property measurement system (PPMS) DynaCool with a 9-T magnet, equipped with a vibrating sample magnetometer (VSM) option. For the resistivity measurements, a standard four-probe technique was used with 20-μm diameter platinum wires attached with silver epoxy. The applied current for these measurements was $I = 2$ mA. Specific-heat measurements were performed with the Quantum Design heat-capacity option, using a relaxation technique. Electron diffraction measurements were performed at Brookhaven National Laboratory on a JEOL ARM200F transmission electron microscope with double-Cs correctors.

ACKNOWLEDGMENTS. This work was primarily supported by the Gordon and Betty Moore Foundation, EPiQS initiative, Grant GBMF-4412. The research performed at the Gdansk University of Technology was financially supported by the National Science Centre (Poland) Grant DEC-2012/07/E/ST3/00584. The electron microscope work done at Brookhaven National Laboratory was supported by the Department of Energy Basic Energy Sciences, by the Materials Sciences and Engineering Division, under Contract DE-AC02-98CH10886.

1. Yeh J-W, et al. (2004) Nanostructured high-entropy alloys with multiple principal elements: Novel alloy design concepts and outcomes. *Adv Eng Mater* 6(5):299–303.
2. Ye YF, Wang Q, Lu J, Liu CT, Yang Y (2016) High-entropy alloy: Challenges and prospects. *Mater Today* 19(6):349–362.
3. Yeh J-W (2013) Alloy design strategies and future trends in high-entropy alloys. *JOM* 65(12):1759–1771.
4. Senkov ON, Miller JD, Miracle DB, Woodward C (2015) Accelerated exploration of multi-principal element alloys with solid solution phases. *Nat Commun* 6:6529.
5. Troparevsky MC, Morris JR, Kent PRC, Lupini AR, Stocks GM (2015) Criteria for predicting the formation of single-phase high-entropy alloys. *Phys Rev X* 5:011041.
6. Youssef KM, Zaddach AJ, Niu C, Irving DL, Koch CC (2016) A novel low-density, high-hardness, high-entropy alloy with close-packed single-phase nanocrystalline structures. *Materials Research Letters* 3(2):95–99.
7. Kou H, Lu J, Li Y (2014) High-strength and high-ductility nanostructured and amorphous metallic materials. *Adv Mater* 26(31):5518–5524.
8. Zou Y, Ma H, Spolenak R (2015) Ultrastrong ductile and stable high-entropy alloys at small scales. *Nat Commun* 6:7748.
9. Gludovatz B, et al. (2016) Exceptional damage-tolerance of a medium-entropy alloy CrCoNi at cryogenic temperatures. *Nat Commun* 7:10602.
10. Gludovatz B, et al. (2014) A fracture-resistant high-entropy alloy for cryogenic applications. *Science* 345(6201):1153–1158.
11. Sharma RG (2015) *Superconductivity - Basics and Applications to Magnets* (Springer, London).
12. Rossi L (2010) Superconductivity: Its role, its success and its setbacks in the Large Hadron Collider of CERN. *Supercond Sci Technol* 23(2010):034001.
13. Kożelj P, et al. (2014) Discovery of a superconducting high-entropy alloy. *Phys Rev Lett* 113(10):107001.
14. Jasiewicz K, Wiendlocha B, Korbeń P, Kaprzyk S, Tobola J (2016) Superconductivity of $Ta_{34}Nb_{33}Hf_8Zr_{14}Ti_{11}$ high entropy alloy from first principles calculations. *Phys Status Solidi Rapid Res Lett* 10(5):415–419.
15. Senkov ON, Scott JM, Senkova SV, Miracle DB, Woodward CF (2011) Microstructure and room temperature properties of a high-entropy TaNbHfZrTi alloy. *J Alloys Compd* 509(20):6043–6048.
16. Bucher E, Müller J (1961) Supraleitung in hexagonalen Ti-V-and Ti-Nb-Legierungen. *Helv Phys Acta* 34:410–413.
17. Collings EW (1983) *A Sourcebook of Titanium Alloy Superconductivity* (Plenum, New York).
18. Graf T, Felser C, Parkin SSP (2011) Simple rules for the understanding of Heusler compounds. *Prog Solid State Chem* 39(1):1–50.
19. Matthias BT (1955) Empirical relation between superconductivity and the number of valence electrons per atom. *Phys Rev* 97(1):74–76.
20. Collver MM, Hammond RH (1973) Superconductivity in amorphous transition-metal alloy films. *Phys Rev Lett* 30(3):92–95.
21. Simon A (1997) Superconductivity and chemistry. *Angew Chem* 36(17):1788–1806.
22. Collver MM, Hammond RH (1977) Reduced superconducting transition temperatures in amorphous transition metal alloys. *Solid State Commun* 22(1):55–57.
23. Mansoori GA, Carnahan NF, Starling KE, Leland TW, Jr (1971) Equilibrium thermodynamic properties of the mixture of hard spheres. *J Chem Phys* 54(4):1523–1525.
24. Takagi H, et al. (1992) Systematic evolution of temperature-dependent resistivity in $La_{2-x}Sr_xCuO_4$. *Phys Rev Lett* 69(20):2975–2978.
25. Gunnarsson O, Calandra M, Han JE (2003) Colloquium: Saturation of electrical resistivity. *Rev Mod Phys* 75(4):1085.
26. Orlando TP, McNiff EJ, Jr, Foner S, Beasley MR (1979) Critical fields, Pauli paramagnetic limiting, and material parameters of Nb_3Sn and V_3Si. *Phys Rev B* 19(9):4545.
27. von Rohr F, Nesper R, Schilling A (2014) Superconductivity in rubidium-substituted $Ba_{1-x}Rb_xTi_2Sb_2O$. *Phys Rev B* 89:094505.
28. Weyeneth S, et al. (2012) Superconductivity and magnetism in $Rb_xFe_{2-y}Se_2$: Impact of thermal treatment on mesoscopic phase separation. *Phys Rev B* 86:134530.
29. Werthamer NR, Helfand E, Hohenberg PC (1966) Temperature and purity dependence of the superconducting critical field. *Phys Rev* 147(1):295.
30. Koch CC, Easton DS (1977) A review of mechanical behaviour and stress effects in hard superconductors. *Cryogenics* 17(7):391–413.
31. McMillan WL (1968) Transition temperature of strong-coupled superconductors. *Phys Rev* 167(2):331.
32. Dynes RC (1972) McMillan's equation and the T_c of superconductors. *Solid State Commun* 10(7):615–618.
33. Allen PB, Dynes RC (1975) Transition temperature of strong-coupled superconductors reanalyzed. *Phys Rev B* 12(3):905.
34. Klimczuk T, et al. (2012) Superconductivity in the Heusler family of intermetallics. *Phys Rev B* 85:174505.
35. Cava RJ, et al. (1988) Superconductivity near 30 K without copper: The $Ba_{0.6}K_{0.4}BiO_3$ perovskite. *Nature* 332:814–816.
36. Hinks G, Richards DR, Dabrowski B, Marx DT, Mitchell AW (1988) The oxygen isotope effect in $Ba_{0.625}K_{0.375}BiO_3$. *Nature* 335:419–421.
37. Shanks HR (1974) Enhancement of the superconducting transition temperature near a phase instability in Na_xWO_3. *Solid State Commun* 15(4):753–756.
38. Testardi LR (1975) Structural instability and superconductivity in A-15 compounds. *Rev Mod Phys* 47(3):637.
39. Hirai D, von Rohr F, Cava RJ (2012) Emergence of superconductivity in $BaNi_2(Ge_{1-x}P_x)_2$ at a structural instability. *Phys Rev B* 86(10):100505(R).